
Algorithm for Optimal Sizing of PV/Wind/Diesel Hybrid Microgrid System Solar Cell Anomaly Detection Based on Wavelet Scattering Transform and Artificial Intelligence

Sabreen Hussein^{1,*} Osama A. Omer² and El-Attar M. Ali²

¹Upper Egypt Electricity Distribution Company, Aswan, Egypt

²Aswan Faculty of Engineering, Aswan University, Abulrish 81542, Aswan, Egypt

Abstract

The detection of the anomalies of the solar cells is done by testing the cells in the lab. However, this method is time consuming and expensive. The analysis of infrared solar cell images can reveal its status by classifying infrared images into anomaly and non-anomaly classes. The anomaly can be due to many reasons. Therefore, it is required to not only classify image into anomaly and non-anomaly, but also, detect the anomaly type. The image-based solar cell anomaly detection methods appearing in the literature used either machine learning or deep learning techniques. The main disadvantages of these methods are the lack of sufficient dataset and/or utilizing inappropriate features for classification. Machine learning requires robust feature extractor which are independent on the imaging condition. On the other hand, deep learning techniques doesn't require feature extractor, however, results depend on the implemented filters in the network i.e the network architecture. In this proposal, we deal with multi-class anomaly detection from infrared images by using better representation of the images features by using Wavelet scattering Transform (WST). The WST coefficients are stable under signal deformations and globally invariant to signal translation and rotation. Based on the simulation results, the proposed method achieved an average accuracy of 99.98%.

Keywords: Solar Cell, Anomaly Detection, Artificial Intelligence, Random Forest, Machine Learning

1. INTRODUCTION

With the increase demand of electrical energy, solar photovoltaic (PV) system, has been rapidly growing in the past decades. The worldwide PV capacity has reached over 500 GW, which increased by 142 GW in 2020 [1]. With the growth of PV systems in the industry, the amount of anomaly PV modules is growing. PV modules are usually suffered from temperature, rain, wind, dust, vegetation etc., which produce damages on the PV modules and mechanical damages during transportations and installations. The damages affect the lifetime of the PV modules. In turn, the damages of PV modules affect to the entire PV system that leads to economic efficiency and energy loss problems. Therefore, it is required to have a fast, reliable, and automatic non-destructive testing method in the inspection and maintenance of the PV modules regularly. Remote sensing of

PV has been attending recently with different approaches such as electroluminescence (EL) images, infrared radiation (IR) images, and RGB images techniques [2]. On the other hand, machine learning and deep learning have been used in the detection and classification process of many applications including solar cell anomaly detection and classification [2,3]. In [4], authors presented deep learning-based photovoltaics fault detection models using thermal images obtained from an unmanned aerial vehicle (UAV) equipped with infrared sensors. The employed models are DeepLabV3+, Feature Pyramid Network (FPN) and U-Net with different encoder architectures. The obtained results revealed intersection over union (IoU) of 79%, 85%, 86%, and dice coefficients of 87%, 92%, 94% for DeepLabV3+, FPN, and U-Net, respectively. However, these models are data dependent.

In [5], Generative Adversarial Network (GAN) which is used in medical domain has been adapted to detect and locate anomalies in the solar cells. This method differentiates between two states of the solar cell: the normal and anomaly cells. Moreover, GAN is effective with the seen dataset which makes it in effective with new data. Also, it is sensitive to the change of the images' features.

In [6], an embedded system for defect detection and diagnosis of PV modules is proposed. Two models have been developed one for fault detection and the other for diagnosis. In the defect detection, authors classify the images into two classes: namely, defected, and non-defected. In this model, they achieved an accuracy of 99%. However, in the diagnosis model, the classify images into four classes and they achieved an accuracy of 95.55%. In [7], a novel system for improved PV diagnostics using drone-based imagery is proposed. This solution consists of three main steps. The first step locates the solar panels within the image by using region selection. The second step detects the anomalies within the solar panels. The final step identifies the root cause of the anomaly. Authors in this work focus on the detection of anomalies within solar panels. They used a region-based convolutional neural network (CNN). This work achieved an accuracy of 90% for the anomaly detection that is two-state classification. On the other hand, wavelet scattering transform (WST) has been proven to be shift, scale and rotation independent. Therefore, it has been effectively used for image classifications. In this paper, WST is used as a feature domain to extract features that are insensitive to scaling and shifting rather than using time domain (TD) [8-13], which is sensitive to scaling, rotation and shifting. Unlike the work done in [2,3], we used the wavelet scattering transform as a feature domain rather than the time domain to make the system more robust against scaling and shifting. WST is used as a feature domain to extract features that are insensitive to scaling and shifting rather than using time domain.

2. THE PROPOSED METHOD

2.1 Preprocessing

The block diagram of the proposed system is shown in Figure 1. The proposed system starts with the dataset partitioning into training, validation, and test dataset. For convenience, these images are transformed into 1D signals. The second stage is the feature domain transformation. In this work, we use WST as the feature domain. Finally, the classification is based on the WST coefficients with ML classifiers. The image-to-signal transformation is done by combining rows sequentially.

2.2. Wavelet Scattering Transform

To compute the WST of a signal x , this signal is processed in three successive operations to

generate wavelet scattering coefficients in each stage. These operations are convolution, nonlinearity, and averaging respectively. Figure 2 displays multiresolution/multilayer wavelet scattering transforms in which the scattering coefficients should be determined at each layer [9-11] as follows:

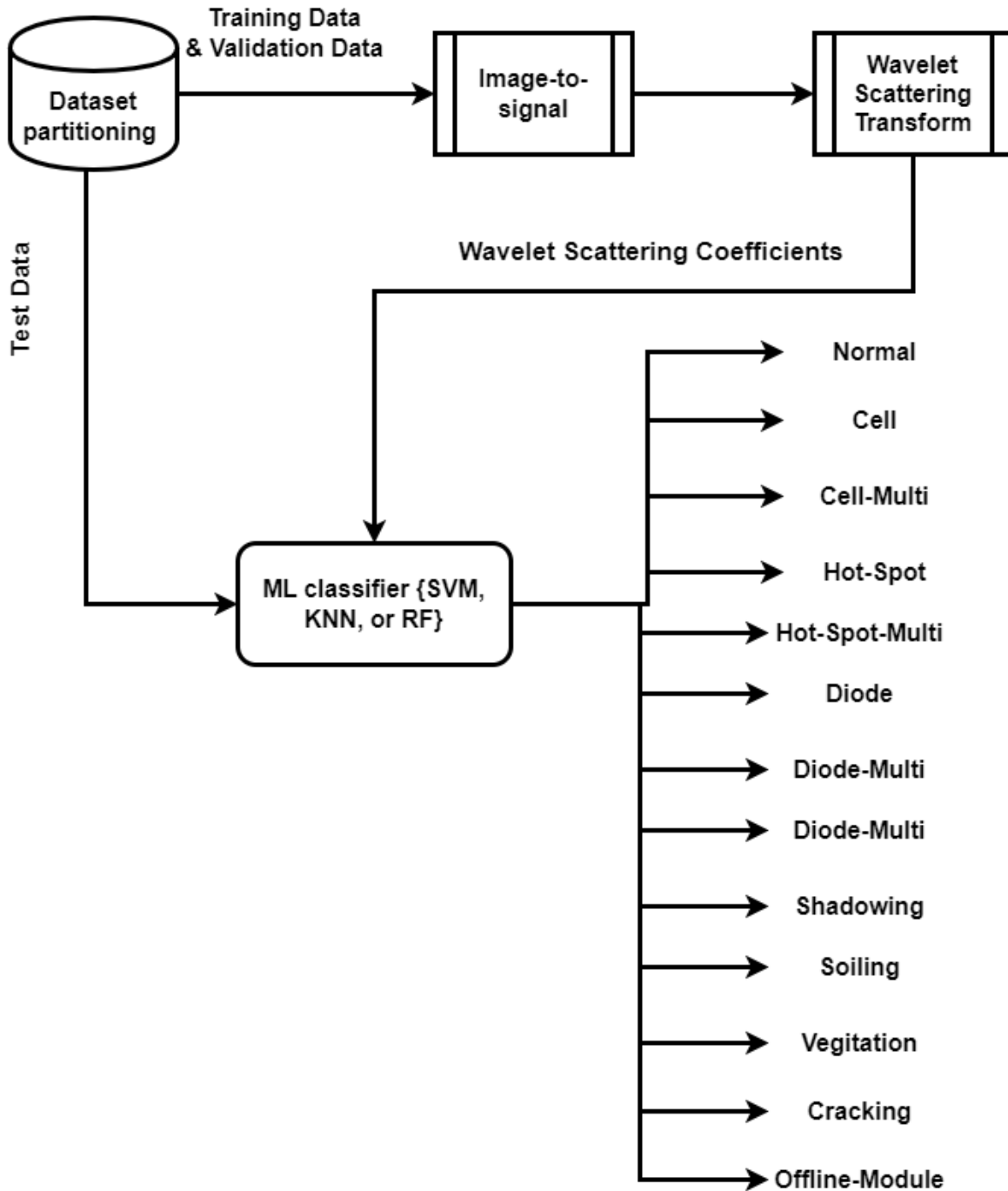


Figure 1: block diagram for the proposed solar cell anomaly detection

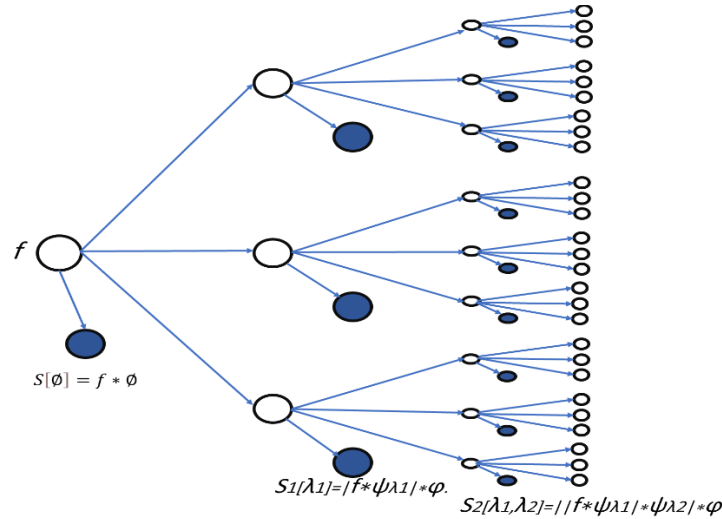


Figure 2: Multilayer wavelet scattering transform.

The zeroth-order scattering coefficients are calculated using basic input averaging as follows:

$$S_0 = x * \phi, \quad (1)$$

where x is the input signal, ϕ is the scaling function, and $*$ is the convolution operator.

The high-frequency bands are captured by convolving with the mother wavelet ψ_{λ_i} at scale λ_i . So, the first-order scattering coefficients, S_1 , are generated by averaging the modules of the lower band at the first scale in the filter bank λ_1 .

$$S_1 x(t, \lambda_1) = |x * \psi_{\lambda_1}| * \phi \quad (2)$$

In the same way, the second wavelet transform is determined as follows:

$$S_2 x(t, \lambda_1, \lambda_2) = |x * \psi_{\lambda_1}| * \psi_{\lambda_2}| * \phi \quad (3)$$

At each step, the signal at the lowest band incurs modules non-linearity and is averaged through the convolution by the father wavelet (low pass) ϕ filter as shown in fig.1. For the m -th layer, the scattering coefficients, S_m , have been computed as follows.

$$S_m x(t, \lambda_1, \dots, \lambda_m) = |x * \psi_{\lambda_1}| * \dots * \psi_{\lambda_m}| * \phi \quad (4)$$

2.3 Artificial Intelligence

Machine learning is a branch of artificial intelligence (AI). The main aim of machine learning is to comprehend the structure of data and fit it into models that people can comprehend and use. A solid prognosis requires fewer medical tests, which makes it important for ML techniques to perform well overall, offer medical professionals with interpretable prognostic information, and enhance decision-making. The main drawback of the ML technique is the requirement of a robust feature extractor. Medical images in spatial domain are not sufficient as a feature for the ML techniques. The results of using ML technique are not acceptable as in [3]. Therefore, the main clue in this proposal is to present WST as a feature domain to be combined with ML to classify infrared images into multi anomaly classes rather than anomaly and non-anomaly images.

On the other hand, deep learning (DL) is a branch of the machine learning. Despite DL doesn't require feature extraction, it requires a huge number of datasets to be efficient. Therefore, to DL has been combined with ML to take the benefit of DL feature extractor [14] and the ML classifier [3]. Even so, the performance of DL-ML classifiers is dependent on the architecture of the DL network. The transfer learning is used also to reduce the required dataset.

2.4 ML Classification Based on WST

As a rotation independent, scaling independent and shift independent, WST is a good candidate for feature extraction. As has been mentioned, the ML classification is highly dependent on the extracted features and its ability to represent the data and differentiate between various classes. Different classifiers are combined with the WST to detect the solar cell anomalies including support vector machine (SVM), k-nearest neighbour (KNN), and random forest (RF).

3. Results of Solar Cell Anomaly Detection

3.1. Dataset

The dataset consists of 20,000 infrared images that are 24 by 40 pixels each. There are 12 defined classes of solar modules presented in this dataset with 11 classes of different anomalies and the remaining class being No-Anomaly (i.e. the null case). In this work, eleven anomalies are differentiated in addition to the no-anomaly case. The different types of anomalies are tabulated in Table 1 [14]. Three examples for each class are shown in Figure 3.

Table 1: The dataset of infrared images

Class Name	Images	Description
Cell	1,877	Hot spot occurring with square geometry in single cell.
Cell-Multi	1,288	Hot spots occurring with square geometry in multiple cells.
Cracking	941	Module anomaly caused by cracking on module surface.
Hot-Spot	251	Hot spot on a thin film module.
Hot-Spot-Multi	247	Multiple hot spots on a thin film module.
Shadowing	1056	Sunlight obstructed by vegetation, man-made structures, or adjacent rows.
Diode	1,499	Activated bypass diode, typically 1/3 of module.
Diode-Multi	175	Multiple activated bypass diodes, typically affecting 2/3 of module.
Vegetation	1,639	Panels blocked by vegetation.
Soiling	205	Dirt, dust, or other debris on surface of module.
Offline-Module	828	Entire module is heated.
No-Anomaly	10,000	Nominal solar module.

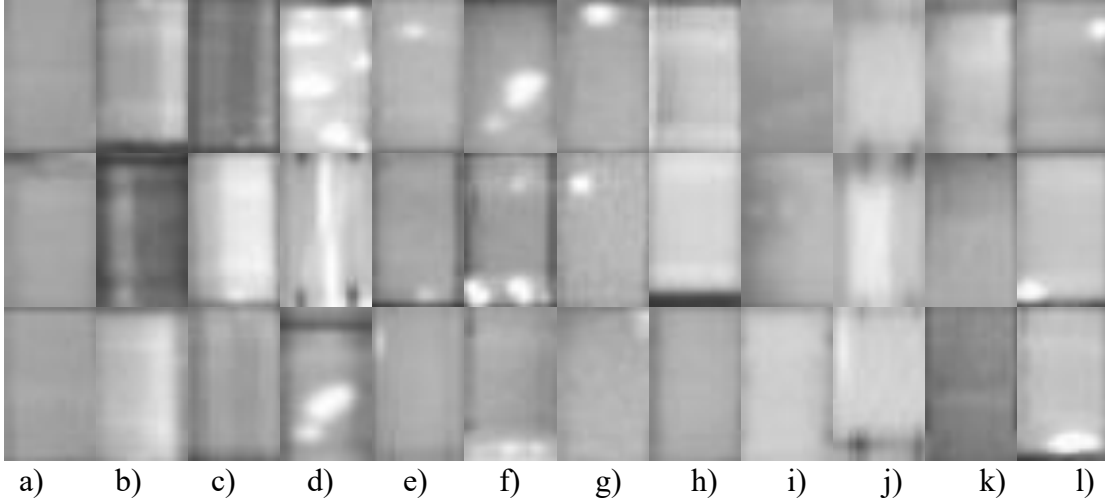


Figure 3: Examples for training images for different classes: a) No-Anomaly, b) Diode, c) Diode-Multi, d) Cracking, e) Cell, f) Cell-Multi, g) Soiling, h) Offline-Module, i) Shadowing, j) Hot-Spot, k) Hot-Spot-Multi, and l) Vegetation classes.

3.2. Implementation Environment

The system used for simulation is CPU Core I5, 2.6 GHz processor on a Windows 10 operating system. The software on which the model is implemented is MATLAB 2022a.

3.3. Performance Metrics

For performance measurement, multiple metrics are utilized, including confusion chart, accuracy, precision, recall, and F1-score. The confusion chart shows the success for each class and confusion with other classes.

The accuracy of the model describes how well the model performs across classes. Accuracy is formulated as shown below. The accuracy can be calculated directly from the confusion chart by dividing the sum of diagonal by the total number of samples

$$Accuracy = \frac{\text{Number of trully classified samples}}{\text{Total number of samples}} \quad (5)$$

Precision is the measure of the models' capability to identify true positives, and it is calculated as shown below. The precession can be calculated from the confusion chart for each column by dividing the value at the diagonal in this column by the summation of that column.

$$Precision = \frac{\text{True Positive}}{\text{True Positive} + \text{False Positive}} \quad (6)$$

The recall is the ratio between the true positive prediction values and the sum of predicted true

positive and false negative values. It is calculated as shown below. The recall can be calculated from the confusion chart for each row by dividing the value at the diagonal in this row by the summation of that row.

$$Recall = \frac{True\ Positive}{True\ Positive + False\ Negative} \quad (7)$$

F1 score is the overall model accuracy that balances precision and recall in a positive class. It is calculated as represented by:

$$F1\ Score = 2 \times \frac{Precision \times Recall}{Precision + Recall} \quad (8)$$

3.4 Experimental Results and Discussion

In this section, we present the simulation results for the infrared images classification using the proposed system compared with the DL method [2]. The comparison is based on four metrics: accuracy, precision, recall and F1-score.

The kernel function used with SVM is Gaussian. The number of classes is four. For the WST, the invariance scale is set to 7, and the sampling frequency is 128.

Table 2 shows the resulting evaluation metrics using different methods. From this table it can be shown that DL network proposed in [2] are efficient in detecting no-anomaly solar cell with high accuracy of 98%, however, it achieved a low accuracy for the overall classification due to the confusion between different type of anomaly (71% 51%, 95%, 91%, 70%, 63%, 82%, 70%, 77%, 28%, and 76%, for Cell, Cell-Multi, Diode, Diode-Multi, Hot-Spot, Hot-Spot-Multi, Cracking, Offline-Module, Shadowing, Soiling, and Vegetation, respectively). Therefore, the average accuracy is 72.67%.

On the other hand, using WST transform results in better images representation and differentiation between different anomalies. Therefore, the combination of WST with the ML networks achieves higher accuracy (99.98%, 74.82% and 74.71% for the case of WST+RF, WST+KNN and WST+SVM networks, respectively) with high precision for the twelve classes.

Another illustrative metric is the confusion chart that can explicitly show the number of confusions with different classes. The confusion charts for different methods are shown in Figure 4a, 4b and 4c. Figure 4c shows that for the three tested classifiers networks, all the non-anomaly images are classified correctly to be non-anomaly so that the precision for the no-anomaly solar cell classification is 100%. In contrast, the proposed WST-based feature extraction achieved less confusion for all anomaly types and non-anomaly images, as shown in Figure 4c.

The high-performance achievement of the WST is due to multiscale contractions, linearization of hierarchical symmetries, and sparse representations. Moreover, WST coefficients are stable under signal deformations and globally invariant to signal translation and rotation.

Table 2, the evaluation metrics for different classification methods

Approach	Classifier	Class	Accuracy (%)	Precession (%)	Recall (%)	F1-Score (%)
Proposed	WST+RF	No-Anomaly	99.98	100	100	100
		Cell		99.97	99.97	99.97
		Cell-Multi		99.70	99.90	99.80
		Diode		99.91	99.85	99.88
		Diode-Multi		100	100	100
		Hot-Spot		99.95	99.98	99.97
		Hot-Spot-Multi		100	100	100
		Cracking		99.92	99.87	99.89
		Offline-Module		100	100	100
		Shadowing		100	100	100
		Soiling		99.96	99.96	99.96
		Vegetation		100	100	100
Proposed	WST+SVM	No-Anomaly	74.71	97.14	76.09	85.34
		Cell		52.85	61.42	56.81
		Cell-Multi		37.75	90.28	53.24
		Diode		44.14	85.48	58.21
		Diode-Multi		63.89	70.64	67.10
		Hot-Spot		51.18	74.86	60.79
		Hot-Spot-Multi		42.87	82.17	56.35
		Cracking		69.53	78.01	73.53
		Offline-Module		38.14	91.123	53.78
		Shadowing		59.80	71.59	65.17
		Soiling		44.09	68.58	53.67
		Vegetation		36.52	87.39	51.51
Proposed	WST+KNN	No-Anomaly	74.82	97.97	75.17	85.07
		Cell		52.40	67.64	59.05
		Cell-Multi		22.49	91.43	36.10
		Diode		54.08	84.31	65.89
		Diode-Multi		63.29	68.34	65.72
		Hot-Spot		53.37	71.57	61.14
		Hot-Spot-Multi		51.54	89.08	65.30
		Cracking		57.21	81.85	67.35
		Offline-Module		19.71	92	32.47
		Shadowing		47.46	67.49	55.73
		Soiling		43.48	75.12	55.08
		Vegetation		24.39	79.92	37.37
[2]	Ensemble	No-Anomaly	98	NA	NA	95
		Cell	71	NA	NA	72
		Cell-Multi	51	NA	NA	56
		Diode	95	NA	NA	96
		Diode-Multi	91	NA	NA	93
		Hot-Spot	70	NA	NA	71
		Hot-Spot-Multi	63	NA	NA	64
		Cracking	82	NA	NA	80
		Offline-Module	70	NA	NA	76
		Shadowing	77	NA	NA	82
		Soiling	28	NA	NA	38
		Vegetation	76	NA	NA	76
	Average	72.67				

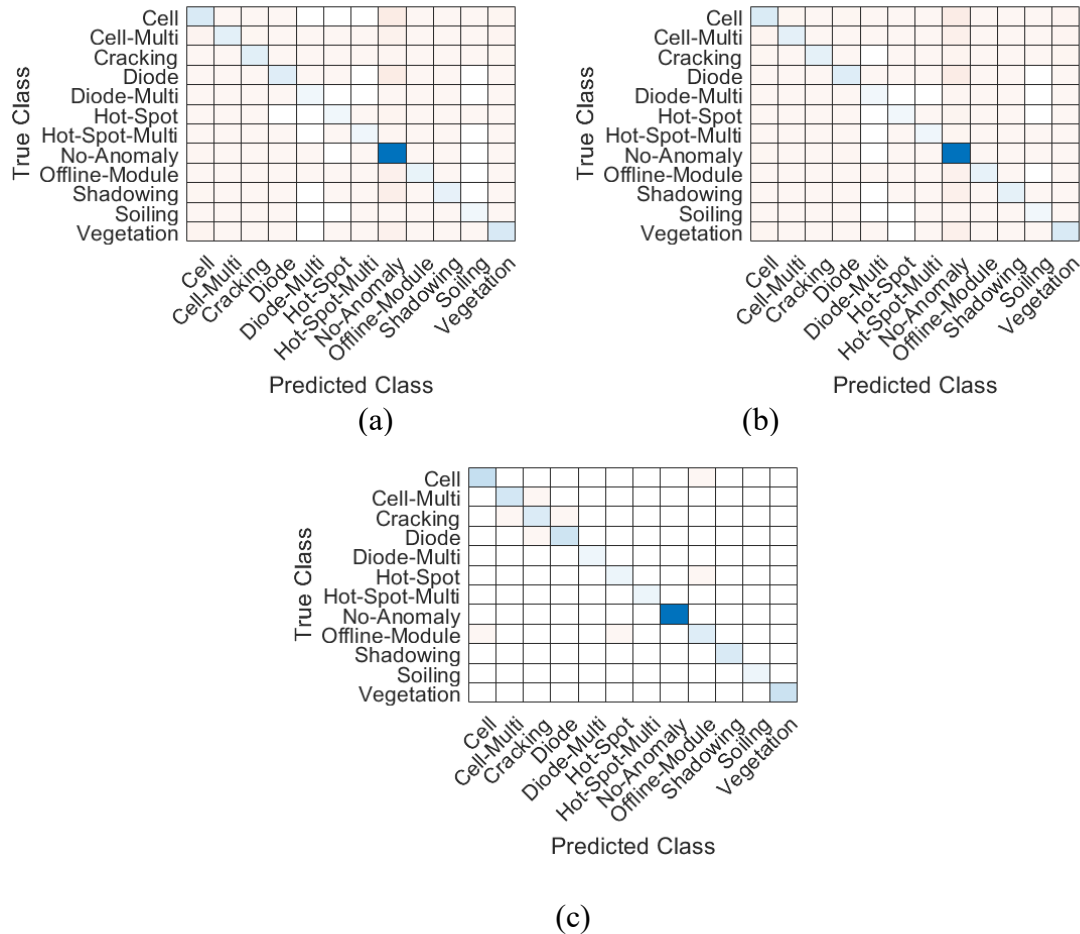


Figure 4, The confusion chart for the anomaly classification based on infrared images using a) SVM, b) KNN and c) RF classifiers in SWT domain

3. CONCLUSION

This work is applying various machine learning techniques for anomaly detection of the solar cell with anomaly type identification. The proposed method is based on the combination of independent transformation that is wavelet scattering transform with the ML classifiers to classify the infrared images into twelve classes. The twelve classes are, Diode, Diode-Multi, Cracking, Cell, Cell-Multi, Soiling, Offline-Module, Shadowing, Hot-Spot-Multi, Hot-Spot, Vegetation and No-Anomaly. Three classifiers are tested with the WST: SVM, KNN and RF. The proposed model WST+RF, outperforms all other methodologies. The performance enhancement of the proposed model is due to the ability of the WST to understand the dataset and extract features from it without being affected by the imaging condition variation. Unlike the work done in the literatures, the proposed model can differentiate between the different types of anomalies effectively.

References

- [1]. Raptor: Raptor Maps Booklet, <https://raptormaps.com/raptor-maps/booklet/>, 2020, last accessed January 2023.

- [2]. Minhuy Le, Van Su Luong, Dang Khoa Nguyen, Van-Duong Dao, Ngoc Hung Vu, Hong Ha Thi Vu, “Remote anomaly detection and classification of solar photovoltaic modules based on deep neural network,” *Sustainable Energy Technologies and Assessments*, Volume 48, 101545, 2021, pp. 1-10.
- [3]. Ali MU, Khan HF, Masud M, Kallu KD, Zafar A, Farhaj Khan Hafiz, Masud Manzar, Kallu Karam Dad, Zafar Amad, “A machine learning framework to identify the hotspot in photovoltaic module using infrared thermography.” *Solar Energy*, 2020, 208:643–51.
- [4]. Jumaboev, S.; Jurakuziev, D.; Lee, M. “Photovoltaics plant fault detection using deep learning techniques.” *Remote Sensing*, No. 14, 3728, 2022, pp. 1-16.
- [5]. Julen Balzategui, Luka Eciolaza and Daniel Maestro-Watson, “Anomaly Detection and Automatic Labeling for Solar Cell Quality Inspection Based on Generative Adversarial Network,” *Sensors* 2021, 21(13), 4361; <https://doi.org/10.3390/s21134361>
- [6]. Adel Mellit, “An embedded solution for fault detection and diagnosis of photovoltaic modules using thermographic images and deep convolutional neural networks,” *Engineering Applications of Artificial Intelligence*, Vol. 116, 2022, 105459, pp. 1-13.
- [7]. Michiel Vlaminck, Rugen Heidbuchel, Wilfried Philips and Hiep Luong, “Region-Based CNN for Anomaly Detection in PV Power Plants Using Aerial Imagery,” *Sensors* 2022, 22, 1244. <https://doi.org/10.3390/s22031244>
- [8]. Soro, B.; Lee, C., “A Wavelet Scattering Feature Extraction Approach for Deep Neural Network Based Indoor Fingerprinting Localization.” *Sensors*, No. 19, 1790, 2019. <https://doi.org/10.3390/s19081790>
- [9]. Mallat, S., “Group Invariant Scattering.” *Communications on Pure Applied Mathematics*, No. 65, 2012, 1331–1398.
- [10]. Bruna, A.; Mallat, S., “Invariant scattering convolution networks.” *IEEE Transaction on Pattern Analysis and Machine Intelligence*, No. 35, 2013, pp. 1872–1886.
- [11]. J. And´en, S. Mallat, “Deep scattering spectrum,” *IEEE Transactions on Signal Processing*, vol. 62, No. 16, 2014, pp. 4114–4128.
- [12]. W. Ghezaiel, L. Brun and O. L´ezoray, "Wavelet scattering transform and CNN for closed set speaker identification," *IEEE 22nd International Workshop on Multimedia Signal Processing (MMSP)*, 2020, pp. 1-6.
- [13]. E. Oyallon, E. Belilovsky, and S. Zagoruyko, “Scaling the scattering transform: deep hybrid networks,” *arXiv preprint arXiv:1703.08961*, 2017
- [14]. Matthew Millendorf, Edward Obropta, and Nikhil Vadhavkar, “Infrared solar module dataset for anomaly detection,” *The International Conf. on Learning Representations*, virtual conference, 2020, pp. 1-5. <https://github.com/RaptorMaps/InfraredSolarModules>